JOURNAL OF PROPULSION AND POWER
Vol. 21, No. 1, January–February 2005

Influence of Hydrogen Addition on Flow Structure in Confined Swirling Methane Flame

Donald M. Wicksall* and Ajay K. Agrawal†
University of Oklahoma, Norman, Oklahoma 73019
and
Robert W. Schefer‡ and Jay O. Keller§
Sandia National Laboratories Combustion Research Facility, Livermore, California 94550

The flowfield of a lean premixed swirl-stabilized burner simulating typical features of land-based gas-turbine combustors was investigated using particle-image velocimetry. Fuel and air were premixed upstream and burned at atmospheric pressure in a quartz-tube combustor operated at a theoretical swirl number of 1.5. Instantaneous-velocity-field measurements were obtained for a nonreacting flow, a methane flame, and a hydrogen-enriched methane flame. Flow measurements were used to obtain two-dimensional vorticity and normal-strain, turbulent-kinetic-energy, and kinetic-energy-dissipation-rate fields. Results show that the average- and instantaneous-velocity fields were affected by the addition of hydrogen to methane. The instantaneous-velocity fields showed smaller eddies that were not present in the time-averaged fields. Higher values of turbulent kinetic energy were observed in the jet region of the methane flame, suggesting the unsteady nature of combustion. The instantaneous vorticity and normal strain were four to seven times higher than the averaged values, indicating the importance of smaller vortical structures to local flame-extinction phenomena.

Introduction

ADVANCED gas-turbine systems utilize lean premixed (LPM) combustion to reduce pollutant emissions. Although LPM systems reduce thermal formation of oxides of nitrogen (NO_x) by lowering the peak flame temperature, they are prone to combustion instabilities, flashback, autoignition, and extinction. Most current LPM combustion systems utilize natural gas, primarily containing methane (CH_4). However, alternative fuels such as gasified coal or biomaterial, chemical, and refinery wastes are driving the need for fuel-flexible gas-turbine systems. Understanding the role of hydrogen (H_2) in LPM combustion of fuels is important for practical applications because many alternative fuels contain significant quantities of H_2. Research on H_2-enriched hydrocarbon fuels is also important as a crossover strategy for the proposed H_2 infrastructure of the future.

One of the first studies of these fuels was conducted by Anderson,[1] who found that H_2 in propane allowed a LPM flame to burn leaner, thereby lowering emissions. More recently, the ability to operate a commercial gas turbine on fuels containing up to 10% H_2 was demonstrated by Morris et al.[2] Nguyen and Samuelson[3] found that a H_2 pilot flame in a LPM combustor significantly improved the extinction performance. An experimental/computational study of H_2 addition to CH_4 was conducted by Ren et al.[4] using single-jet wall stagnation flow and symmetric, opposed-jet flow configurations. They found that fundamental properties such as laminar flame speed and flammability limit did not fully explain the combustion performance of H_2-enriched fuels. Instead, the effect of fluid mechanics, manifested by the induced strain rate, was necessary to characterize the combustion of H_2-enriched fuels. A similar study in opposed-jet flow configuration by Jackson et al.[5] showed that enriching CH_4 with H_2 increased the maximum allowable strain rate before extinction temperatures were reached.

Although simplified configurations[4,5] permit isolation and evaluation of particular combustion phenomena, practical gas-turbine systems involve complexities such as swirl, flow recirculation, shear and boundary layers, and turbulence. Thus, Schefer et al.[6] conducted experiments in an enclosed swirl-stabilized combustor representing geometric features of advanced gas turbines. They found that addition of H_2 to CH_4 extended the flame stability and lean blowoff limit for a range of reactant flow rates. The OH planar laser-induced fluorescence (PLIF) images revealed broader and more intense reaction zones when H_2 was added to CH_4. For a given chemical energy input, the H_2-enriched flame was shorter and more intense. The results provided evidence that the LPM flame structure was influenced by the fuel composition. Because of the strong coupling between the flame structure and flowfield, one would also expect fuel composition to affect the combustor fluid dynamics. Thus, the motivation of the present study is to investigate the influence of H_2 addition on the flowfield in a confined, swirl-stabilized combustor operated on CH_4. Of particular interest is the transient flow structure affecting phenomena such as combustion stability and flame blowoff.

Swirling flows have been studied extensively for many years, without and with combustion. However, most of these studies have yielded the flow structure in terms of mean and root-mean-square (rms) velocities.[7] Recently, Ji and Gore[7] employed particle image velocimetry (PIV) to obtain instantaneous and time-averaged flowfields in an unconfined swirl-stabilized burner, with and without combustion. Many smaller-scale vortices were observed in the instantaneous flowfields in contrast to the averaged field with a single large vortex. The vorticity magnitude in the flame was significantly higher than that in the nonreacting flow. Based on the differences in the mean- and instantaneous-flow structures, they proposed that the latter should be used to evaluate transient LPM combustion phenomena.

Archer and Gupta[8] investigated the effects of combustion and confinement in swirling flames using a stereoscopic PIV system to obtain three-dimensional flowfield data. They reported that combustion affected the size and extent of the recirculation zone as well

Received 30 July 2003; revision received 2 April 2004; accepted for publication 1 May 2004.

*Graduate Assistant, Department of Aerospace and Mechanical Engineering.
†Wayd E. and Joyce Austin Presidential Professor and Associate Professor, Department of Aerospace and Mechanical Engineering; aagrawal@ou.edu. Senior Member AIAA.
‡Senior Member of Technical Staff, Hydrogen and Combustion Technologies. Senior Member AIAA.
§Department Manager, Hydrogen and Combustion Technologies. Senior Member AIAA.

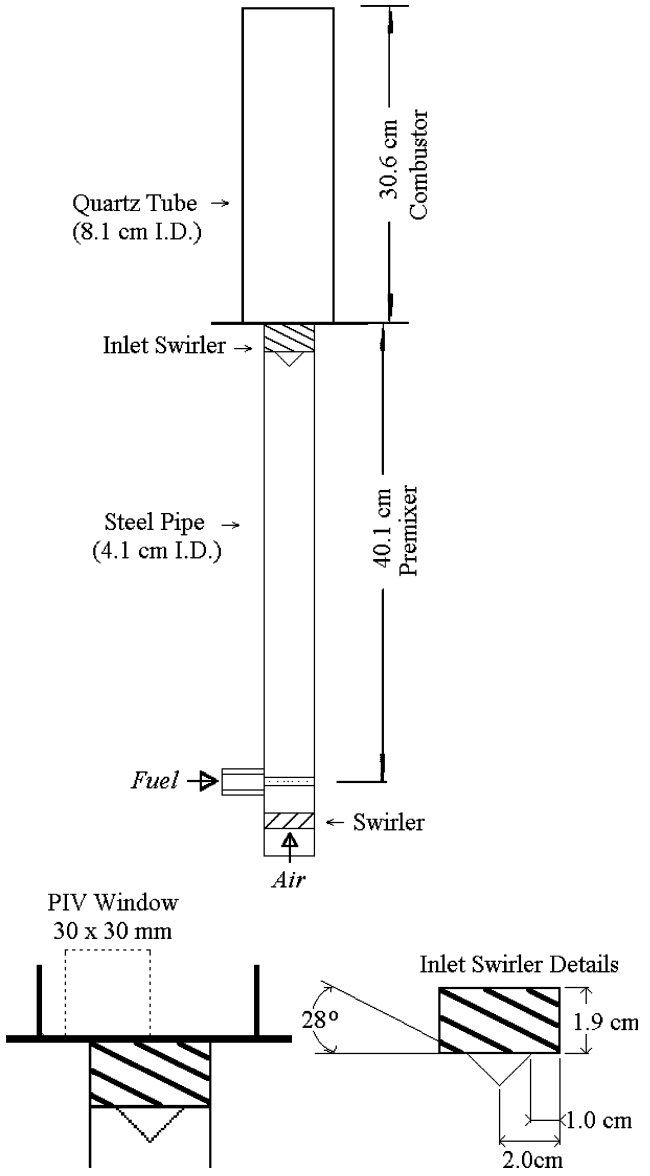

Fig. 1 Schematic of the burner and premixer sections.

as the flow and vorticity fields. The confinement produced a shorter and thicker recirculation zone, although these observations were limited to the nonreacting flow. Griebel et al.[9] used PIV to measure the nonreacting flowfield in a high-pressure combustor and obtained turbulence intensities and integral length scales. Studies have also been conducted to obtain simultaneous measurements of the flowfield using PIV and the reaction zone using OH or CH PLIF.[10,11] These studies provide direct evidence of interactions between the flowfield and the flame behavior, which may be used to develop relevant correlations. However, such measurements are difficult to obtain, especially in the confined swirling flames considered in the present study.

This review indicates that instantaneous PIV measurements in swirling flows have only been obtained for 1) unconfined flows without/with LPM combustion[7,8] and (b) confined flows without combustion.[8,9] Furthermore, none of the past studies have considered effects of fuel composition on instantaneous flowfield in LPM swirling combustion. Thus, the objective of this research is to investigate how the instantaneous and time-averaged flowfields of a flame are affected by the fuel composition. Experiments involve an enclosed swirl-stabilized burner operated on CH_4 and H_2-enriched CH_4. Several flow properties derived from PIV measurements such as average and rms velocities, two-dimensional vorticity and normal strain, turbulent kinetic energy, and kinetic-energy dissipation rate will be presented to reveal the changes in the flowfield when CH_4 is enriched with H_2. Flow properties in reacting flows will be compared with those in a nonreacting flow.

Experimental Approach

Figure 1 shows a diagram of the combustor and premixer sections, with details of the swirler and the PIV measurement region. The burner replicates important geometric features of land-based gas-turbine combustion systems, for example, a premixed swirling flow expanding into an enclosure. The fuel was injected from a spoke located downstream of an air swirler to enhance mixing. The premixer was a 40.1-cm-long 304-stainless steel tube with an inside diameter (i.d.) of 4.1 cm. The combustor was operated with air at atmospheric temperature and pressure. Hydrogen and CH_4 (99% purity) were utilized as fuels, and the combustor was fired at 15–20 kW. A handheld propane torch was used to ignite the reactants at the combustor exit.

The fuel/air mixture issued into the combustion chamber through a set of six axial swirl vanes located in the annulus between the center body and the wall of the premixer section. Figure 1 also shows a detailed drawing of the inlet swirler. The vanes were angled

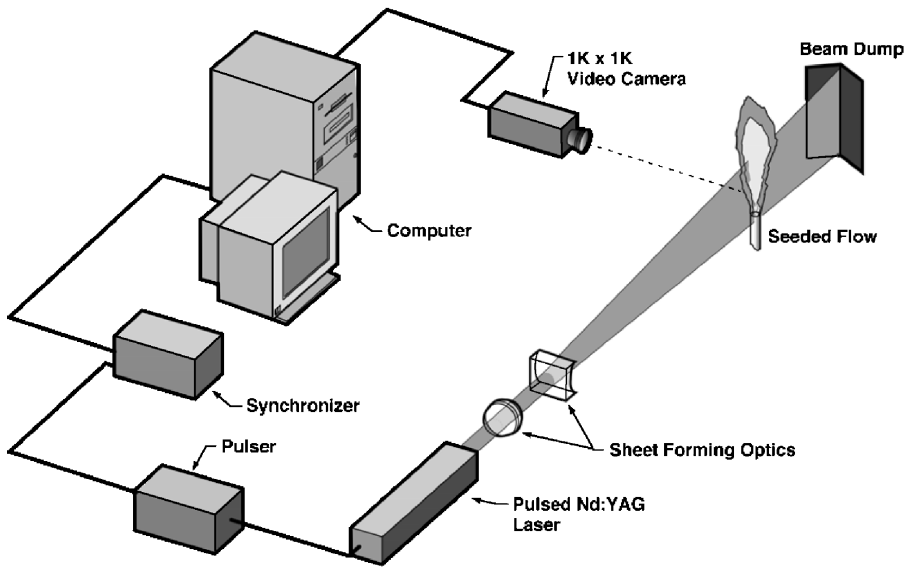

Fig. 2 Schematic of the PIV imaging system used in this experiment.

at 28 deg from the horizontal and the annulus had inside and outside diameters of 2.0 and 4.1 cm, respectively. The bulk axial velocity through the inlet annulus was constant for all cases at 10 m/s, which resulted in an inlet Reynolds number of approximately 13.5×10^3. Equation (1) was used to calculate the swirl number as defined by Gupta et al.,[12]

$$S = \frac{2}{3} \cdot \left[\frac{1 - (d_h/d)^3}{1 - (d_h/d)^2} \right] \cdot \tan\phi \tag{1}$$

where d_h is the centerbody diameter, d is the swirler diameter, and ϕ is the swirler vane angle measured from the axis. The swirl number calculated from Eq. (1) is 1.5.

A 30.6-cm-long quartz glass tube with i.d. 8.1 cm and outside diameter (o.d.) 9.1 cm was used as the combustion chamber. Quartz glass was used because of its ability to withstand high temperatures and transmit ultraviolet light. Reflections of the incoming laser beams from the back of the quartz tube were problematic because the detection wavelength is the same as the laser wavelength for PIV. To alleviate this problem, half of the inside of the quartz tube was sandblasted.

Experiments were conducted with a nonreacting flow, a CH_4 flame, and an H_2-enriched CH_4 flame. The H_2-enriched fuel consisted of 40% H_2 and 60% CH_4 by volume. The calculated adiabatic flame temperature was held constant at $1350 \pm 20^\circ$C to compare flames at a given engine power. The operating parameters were chosen such that the CH_4 flame was close to the unstable region, where H_2 addition is expected to provide the greatest stabilizing effect. Table 1 lists the fuel and air flowrates at the test conditions.

Velocity measurements were obtained using the PIV system shown schematically in Fig. 2. The light source was a double-oscillator-chamber ND:YAG laser (Spectra Physics PIV 400) providing 400 mJ/pulses at 532 nm with a repetition rate of 10 Hz. A cylindrical and a spherical lens were used to form a vertical light sheet 50 mm high and 0.5 mm thick. The time delay between the two PIV pulses was 15 μs. The laser-sheet thickness and pulse delay were chosen to minimize lost particle pairs due to the strong out-of-plane velocity component associated with swirling flows.[7] Ceramic spheres with a nominal diameter of 1.6 μm were used for seeding. The particles were added to the airflow in a fluidized bed seeder upstream of the premixer. A cyclonic separator was used to remove agglomerations of particles to achieve a sufficiently uniform particle-size distribution.

Table 1 Test conditions for the experiment

Variable	CH_4 fuel	H_2-enriched fuel
Total flow rate (SLM)	584.0	584.0
Air flow rate (SLM)	550.5	538.6
CH_4 flow rate (SLM)	33.5	27.3
H_2 flow rate (SLM)	0.0	18.1
Equivalence ratio	0.58	0.56

Images of Mie-scattered light from the seed particles were recorded utilizing a digital camera. The camera (TSI Model 630045 cross-correlation camera) had a 1024 by 1024 pixel image and was placed normal to the laser sheet. An f2.8 lens with a 105-mm focal length was used to collect the scattered light, and the field of view was 30 by 30 mm. Background light and flame luminescence were removed using a 10-nm bandpass filter centered at 532 nm. The two images were recorded on sequential frames to allow a cross-correlation analysis of the data.

The data were analyzed using PIV LAB 2000 (version 1.50) Matlab routines.[13] This program utilized an iterative algorithm to improve the spatial resolution and decrease the number of incorrect vectors. The first two iterations of the solver used a 64 by 64 pixel region to obtain initial values, and the next five iterations had a 32 by 32 pixel interrogation region, which corresponds to a spatial resolution of 0.9 mm. The interrogation regions were 50% overlapped, resulting in a distance between vectors of 0.45 mm. The pixel displacements were converted to units of m/s using the measured field of view and the time between pulses.

Data Analysis

The measured data were filtered to remove outliers using the three-standard-deviation test for both the average and rms velocity values. As expected, the noise in the rms field was reduced, whereas the average field remained relatively unchanged. In this study, at least 200 images were taken for each experiment to ensure accurate data analysis. The computed values were independent of the number of images for image sets greater than 100.

The PIV measurements were used to obtain the two-dimensional planar vorticity, given as

$$\omega_z = \frac{\partial v}{\partial x} - \frac{\partial u}{\partial y} \tag{2}$$

where x and u are, respectively, the coordinate and velocity in the radial direction and y and v are, respectively, the coordinate and velocity in the axial direction. Note that the remaining two components of the vorticity could not be obtained from the monoscopic PIV data taken. The two-dimensional normal strain is given as

$$\varepsilon_{2D} = \frac{\partial u}{\partial x} + \frac{\partial v}{\partial y} \tag{3}$$

A path-integration method was chosen to differentiate the velocity data in Eqs. (2) and (3). This was necessary because the velocity vectors had a 50% overlap, which meant that neighboring data were 50% correlated. The path-integral method utilized a square boundary defined by the eight surrounding data points.[14] The uncertainty of the velocity measurements was calculated following the work of Haste.[15] The uncertainty in the velocity measurements is 0.31 m/s, corresponding to 3.1% of the average axial velocity at the combustor inlet. The uncertainty for the vorticity and normal strain, calculated as 0.61 times the error in the velocity divided by the distance between velocity vectors,[14] is 400 s^{-1}.

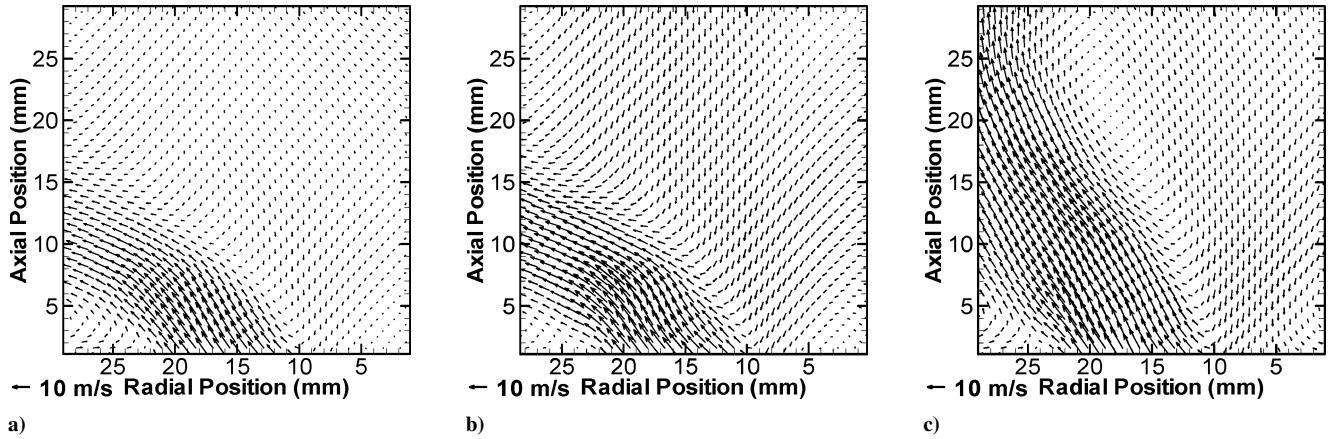

Fig. 3 Time-averaged velocity field for a) nonreacting case, b) CH_4 flame, and c) H_2 enriched flame.

Results and Discussion

The operating conditions were plotted onto a modified turbulent-combustion diagram[16] to reveal that the CH_4 flame was in between the wrinkled and thickened–wrinkled regimes, and the H_2-enriched flame was in the thickened–wrinkled regime. The estimated Kolmogorov length scale varied between 0.01 and 0.2 mm, whereas the estimated Taylor microscale ranged from 0.1 to 2.0 mm. The spatial resolution of 0.9 mm in the present study was inadequate to capture the smallest length scales. However, the measurements resolved only the larger structures in the Taylor microscale. Several aspects of the flowfields of the flames and the nonreacting flow are presented next to show the differences in the flowfields caused by heat release and H_2 addition.

Time-Averaged Velocity Fields

Figure 3 shows time-averaged velocity vectors for the 30 by 30 mm window indicated in Fig. 1. For clarity, only 25% of the vectors are shown; vectors failing the three-standard-deviation outlier test were not averaged. The right side of the image corresponds to the combustor centerline, and the bottom edge is the inlet plane. The inlet annulus is located between radial coordinates of 10 and 20 mm and is denoted by the high jet velocity. The combustor wall is outside the field of view. Vectors failing the three-standard-deviation outlier test were not averaged. Five distinct regions of the flow, similar to those in previous studies, are observed in Fig. 3. The first region is the inlet jet flow directed downstream and radially outward in the combustor. The sudden expansion causes circulation to develop at the intersection of the combuston-inlet plane and the combustor wall, which is referred to as the corner recirculation zone. The central region of the combustor in backflow is the central recirculation zone. The fourth region is the inner shear layer formed between the inlet jet and the central recirculation zone. Finally, an outer shear layer is present between the inlet jet and corner recirculation zone.

An examination of Fig. 3 reveals differences in the time-averaged flowfields of nonreacting flow, CH_4 flame, and H_2-enriched CH_4 flame. The flow velocities in the central recirculation region are on the order of 1–2 m/s for the nonreacting case. However, in the case of flames, the flow velocities in this region are on the order of 3–4 m/s. The heat release that is associated with combustion results in volumetric expansion to accelerate the flow, thereby leading to

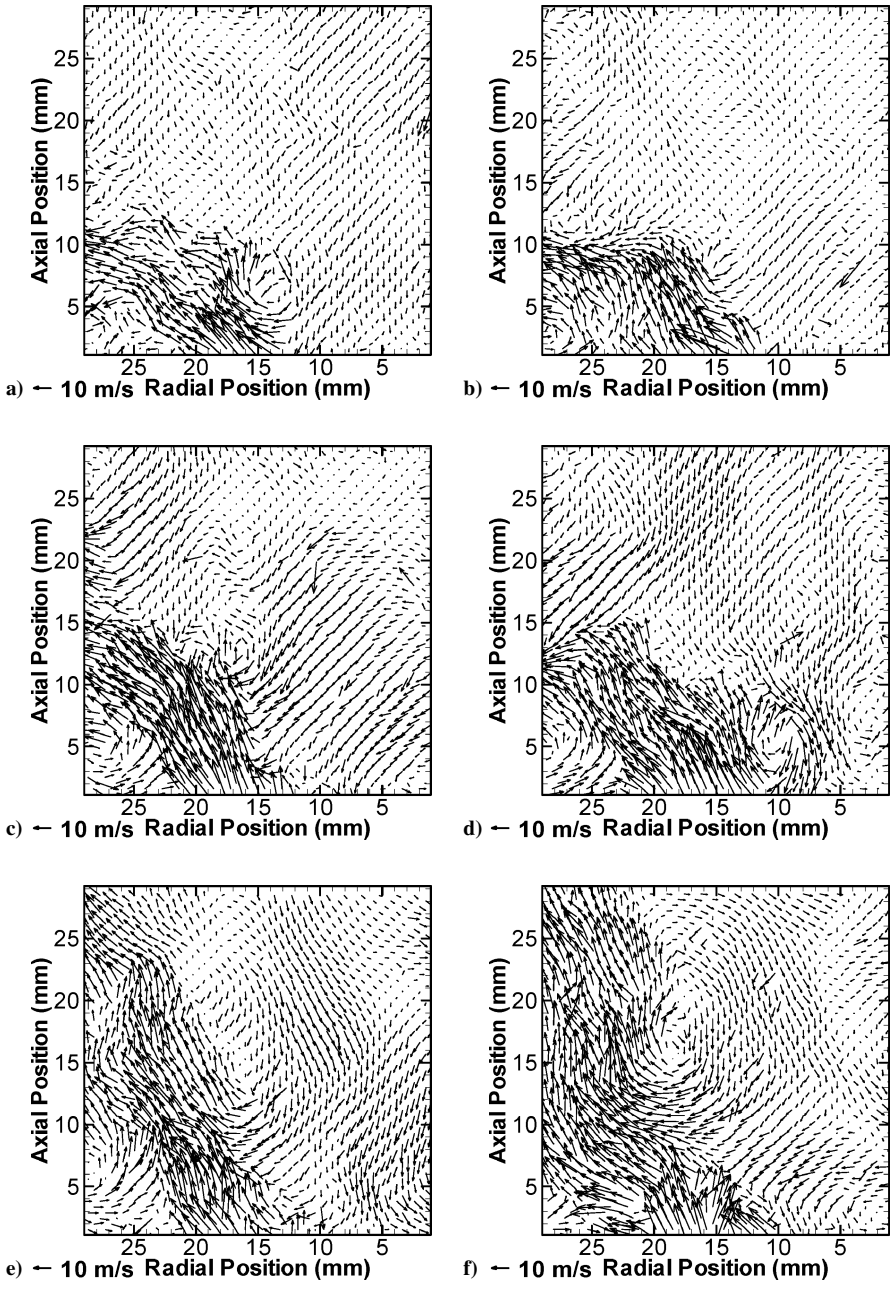

Fig. 4 Instantaneous-velocity fields at random times for a) and b) nonreacting case, c) and d) CH_4 flame, and e) and f) H_2-enriched flame.

higher velocities in the central recirculation zone. Figure 3 shows that the size of the central recirculation zone is about the same for the nonreacting flow and CH_4 flame. A slightly narrower recirculation region is observed for the H_2-enriched flame. These results differ from those in the unconfined configuration of Ji and Gore.[7] In an unconfined system, the heat released in the flame expands the flow in the radial direction to produce a wider central recirculation zone. In the present configuration, the radial expansion is constrained by the combustor wall.

Figure 3 shows that the jet region is similar for the nonreacting flow and CH_4 flame. In both cases, the jet is oriented at approximately a 45-deg angle with respect to the combustor inlet plane. This result suggests that the CH_4 flame is unable to sustain combustion in the highly strained jet region, where conditions similar to the nonreacting flow are maintained. Reactions are primarily confined to the inner shear layer, where thermal expansion has produced higher flow velocities compared to the nonreacting flow. The jet-flow structure for the H_2-enriched flame is significantly different from the previous two cases. The jet region is broader and it is oriented at a 60-deg angle with respect to the combustor inlet plane. Increased momentum caused by the heat release in the jet region would explain this observation, suggesting that the H_2-enriched flame is able to sustain combustion in the highly strained jet region. Figure 3 shows that a corner recirculation region is present for all cases, although full visualization was constrained by the limited field of view. The corner recirculation zones for the nonreacting flow and CH_4 flame are similar, indicating lack of reaction in this region, in agreement with flame luminosity and OH PLIF measurements by Schefer et al.[6] Flow velocities in the corner recirculation zone are higher for the H_2-enriched flame, indicating thermal expansion in the presence of reactions. Overall, results presented in Fig. 3 provide direct evidence that the average flow structure is affected not only by combustion but also by the fuel composition, which determines the location and rates of heat release.

Instantaneous Velocity Fields

Figure 4 shows instantaneous velocity vectors at two random instants of time for the three cases. For clarity only 25% of the vectors

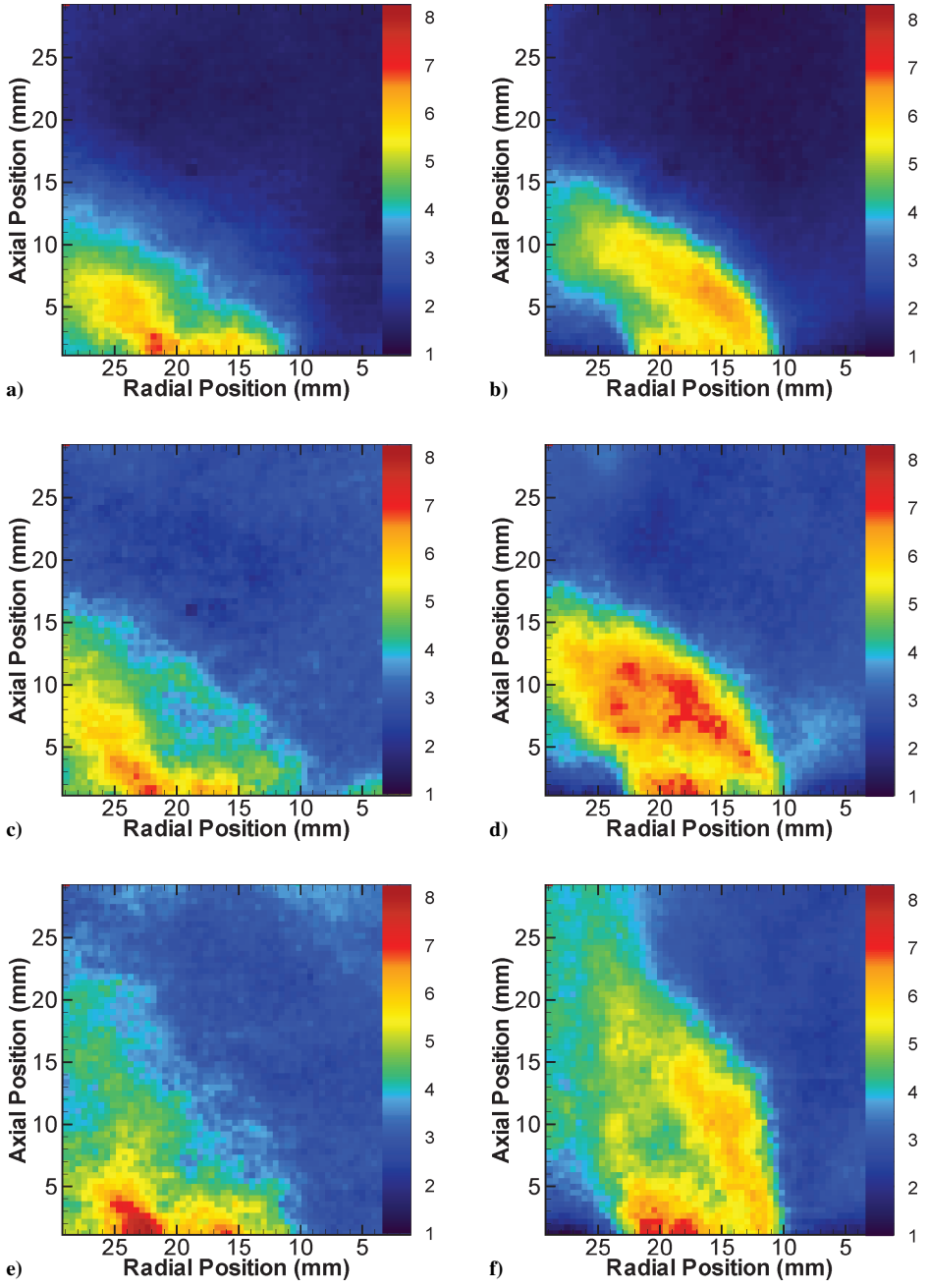

Fig. 5 Radial rms velocity (left column), and axial rms velocity (right column) fields in units of m/s for a) and b) nonreacting case, c) and d) CH_4 flame, and e) and f) H_2-enriched flame.

are shown. In each case, significant temporal variations are observed because of the turbulent nature of the flow. The instantaneous flowfield for the nonreacting case in Figs. 4a and 4b shows that the velocity magnitudes are similar to those observed in the time-averaged flowfield. One major difference is the smaller vortical structures not observed in the averaged flowfield. The recirculation zones observed in the averaged flowfield are still present. According to Figs. 4c and 4d, the magnitude of the velocities in the CH_4 flame is higher than the magnitude in the nonreacting flow, most notably in the central recirculation region. Smaller vortical structures observed later in the inner shear are expected to affect the flame stabilization. For the H_2-enriched flame, the inlet jet in Figs. 4e and 4f is observed to have shifted noticeably downstream, as in the time-averaged flowfield. Overall, results in Fig. 4 show that the average flowfield does not represent the instantaneous flowfield, which contains random smaller vortical structures. Thus, instantaneous flow measurements are necessary to characterize flame properties in a turbulent flow.

Turbulence Fields

Figure 5 shows plots of the rms velocity fields for the three cases. For all cases, the radial rms velocity peaks in the outer shear layer at the inlet plane, where turbulent fluctuations cause the flow to shift between the inlet jet and corner recirculation zone. The axial rms velocity fields show a peak in the inner shear layer for similar reasons. Peak rms values in the nonreacting flow are 6 to 7 m/s, and the rms values in the central recirculation region are around 1 m/s (Figs. 5a and 5b). In general, higher mean velocities have led to higher magnitudes of rms velocity in the inlet jet region. Figures 5c and 5d show a broad region of high axial rms velocity in the inlet jet of the CH_4 flame, indicating the unsteady nature of the heat release. The unsteady heat release causes intermittent flow acceleration to produce large flow fluctuations. The rms velocities in the central recirculation zone are higher, between 2 and 3 m/s, compared to the nonreacting flow. For the H_2-enriched flame, the downward shift of the inlet jet is reflected in the rms velocity fields. The rms velocity is highest in the shear layers on either side of the inlet jet because of the vortical structures in these regions. The rms velocities in the central recirculation region are similar to the CH_4 flame. The broad region of high rms axial velocity in the inlet jet region observed

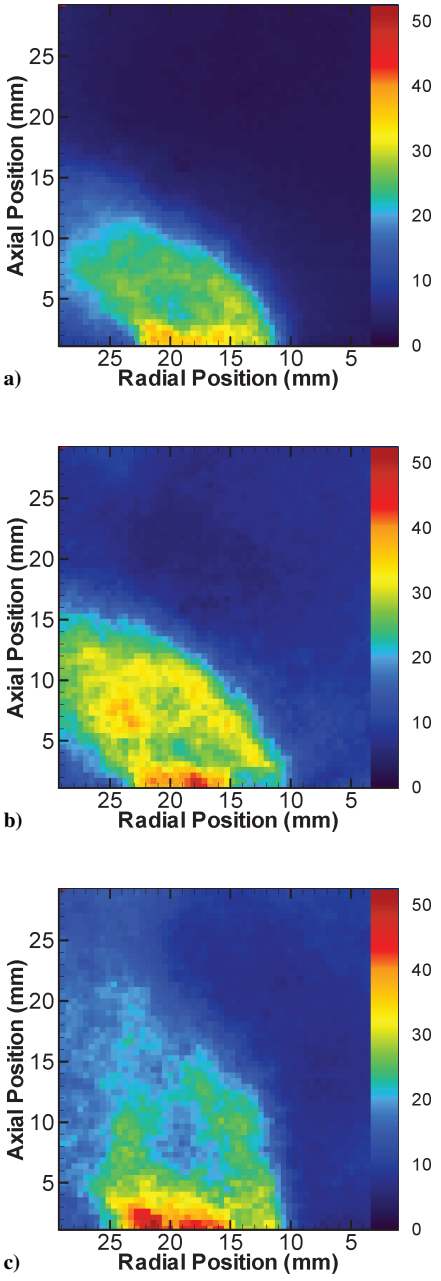

Fig. 6 Turbulent kinetic energy plots for a) nonreacting case, b) CH_4 flame, and c) H_2-enriched flame.

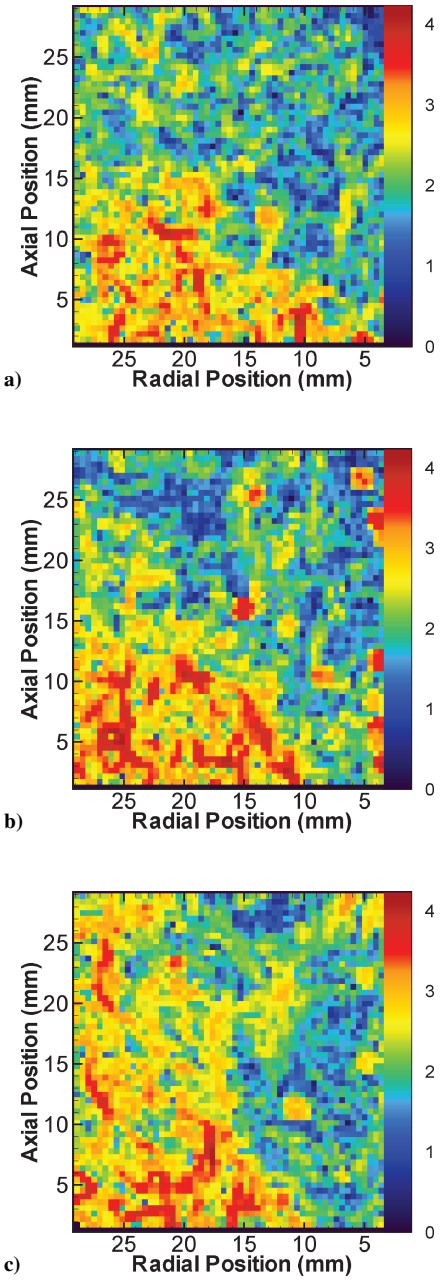

Fig. 7 Two-dimensional kinetic-energy dissipation rate plots in units of m^2/s^3 for the instantaneous-velocity fields shown in the left column of Fig. 4 as Log_{10} values: a) nonreacting case, b) CH_4 flame, and c) H_2-enriched flame.

for the CH_4 flame is not present. This suggests steady heat release, producing a more robust flame for the H_2-enriched fuel.

Next, the turbulent kinetic energy (TKE) was calculated using

$$\mathrm{TKE} = \tfrac{1}{2}\left(U_{\mathrm{rms}}^2 + V_{\mathrm{rms}}^2\right) \tag{4}$$

where the out-of-plane rms velocity is not considered. Figure 6 shows that the TKE is maximum near the inlet jet and minimum in the central recirculation region. These trends are related to the mean and rms velocity magnitudes in the inlet-jet and central-recirculation regions. Much of the TKE is confined to the inlet-jet region, where the velocity is the highest. In the CH_4 flame, higher levels of TKE in the inlet-jet region signify the unsteady nature of combustion, an observation also made from rms velocity plots in Fig 5. Higher TKE levels observed in the inlet-jet region of the CH_4 flame are not present in the H_2-enriched flame. In the H_2-enriched flame, more stable combustion reduces velocity fluctuations and, hence, the TKE. Unlike the measurements of Ji and Gore,[7] the maximum TKE is about the same for the nonreacting and reacting flows. The increase in the TKE in the unconfined geometry of Ji and Gore[7] may be attributed in part to the entrainment of the surrounding air by the reacting flow. Such entrainment is absent in the present study because of confinement by the combustor wall.

Kinetic-energy dissipation rate is a measure of the conversion of the kinetic energy of the flow to internal energy of the fluid by viscous losses at small scales. The two-dimensional kinetic-energy dissipation rate was defined as follows:

$$\varepsilon_{2\mathrm{D}} = 2\nu\left[\left(\frac{\partial u}{\partial x}\right)^2 + \left(\frac{\partial v}{\partial y}\right)^2 + \frac{1}{2}\left(\frac{\partial u}{\partial y} + \frac{\partial v}{\partial x}\right)^2\right] \tag{5}$$

where ν is the kinematic viscosity of the fluid, assumed to be air under atmospheric conditions.[17]

The two-dimensional kinetic-energy dissipation rate for instantaneous-velocity fields is shown in Fig. 7 using the Log_{10} scale. A majority of the structures in Fig. 7 are strand-shaped, representing two-dimensional projections of dissipation around three-dimensional vortical structures. Intense energy dissipation occurs in the inlet-jet and corner-recirculation zones, where the velocity is high. The kinetic-energy-dissipation-rate field for the CH_4 flame is similar to that in the nonreacting case, because of the similarity in the flow structure. In the H_2-enriched flame, the region with high

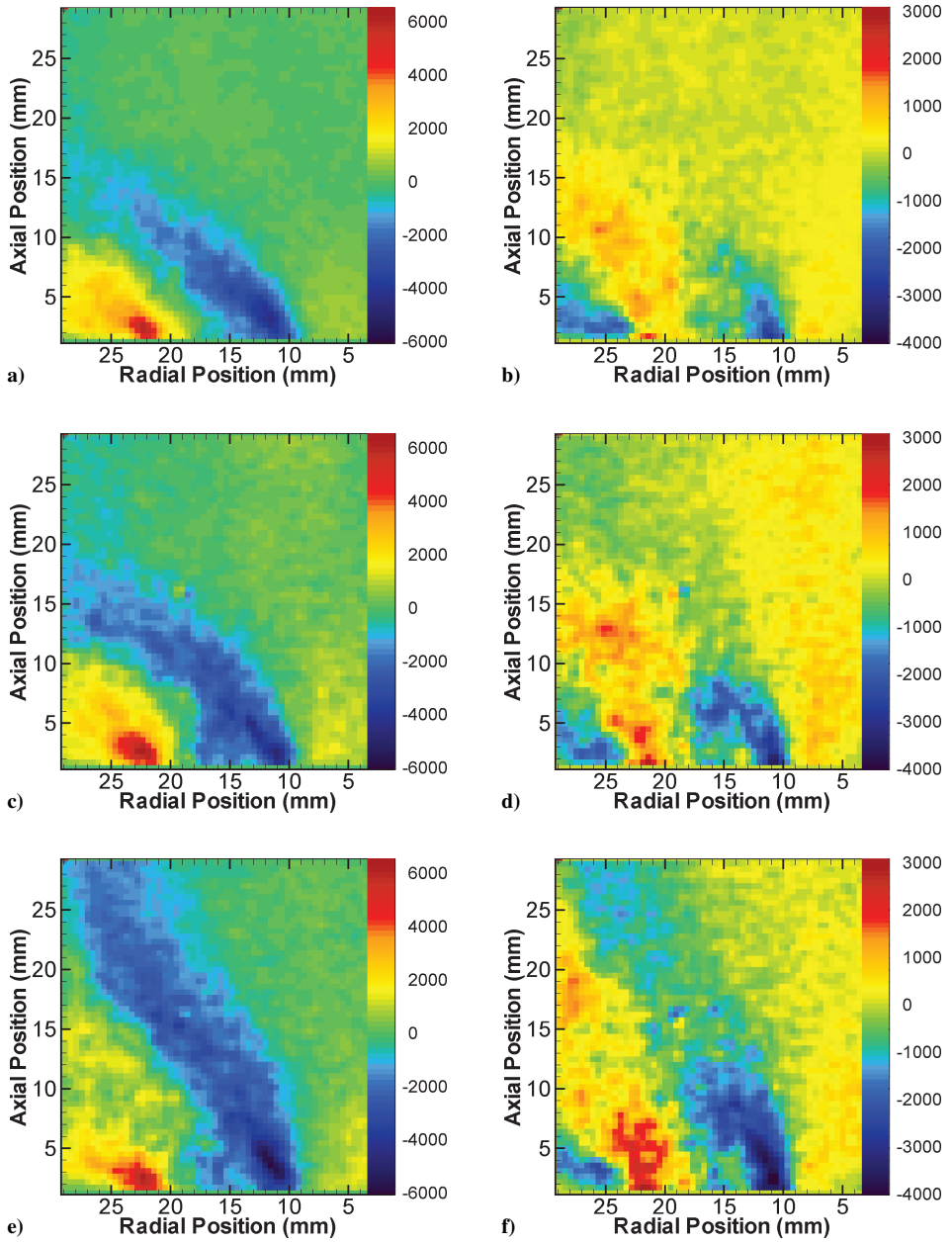

Fig. 8 Vorticity (left column) and normal strain (right column) plots of the average velocity field in units of 1/s: a) and b) nonreacting case, c) and d) CH_4 flame, and e) and f) H_2-enriched flame.

values of kinetic-energy dissipation rate has shifted downstream because of the change in the orientation of the inlet jet region.

Two-Dimensional Vorticity and Normal Strain Fields

Figure 8 shows the vorticity and normal strain calculated from the average velocity fields for the three cases. Negative vorticity is observed in the inner shear layer where the reverse flow turns clockwise to join the inlet jet. The region of positive vorticity is associated with the counterclockwise rotating flow in the corner recirculation zone. For the nonreacting case (Fig. 8a), peak vorticity magnitudes of about 5000 s^{-1} are observed in the shear layers, whereas the vorticity magnitudes in the central recirculation region are relatively low. Peak vorticity values in the shear layers of the CH_4 flame (see Fig. 8c) have increased to 6000 s^{-1} because of higher velocities in the flame. In the case of the H_2-enriched flame, the regions of high vorticity are broader and shifted upward in conjunction with the shear layers. The peak vorticity values are similar to those for the CH_4 flame.

The averaged normal strain data for the three cases are also shown in Fig. 8. Normal strain is important because compression promotes combustion, whereas expansion may cause flame extinction. Figure 8b for the nonreacting case shows that the regions of negative strain or compression are located in the inner shear layer and corner-recirculation zone. Positive strain or expansion is observed in the outer shear layer. Normal strain is generally small in the central recirculation region. The peak values for the normal strain are 2000 s^{-1} in compression and 1000 s^{-1} in expansion. Figure 8d shows the average normal strain for the CH_4 flame. Although the general features are similar to those in the nonreacting case, the magnitudes of normal strain have increased. The peak values are 3000 s^{-1} in compression and 2000 s^{-1} in expansion. The higher extensional strain rate is caused by the volumetric expansion associated with

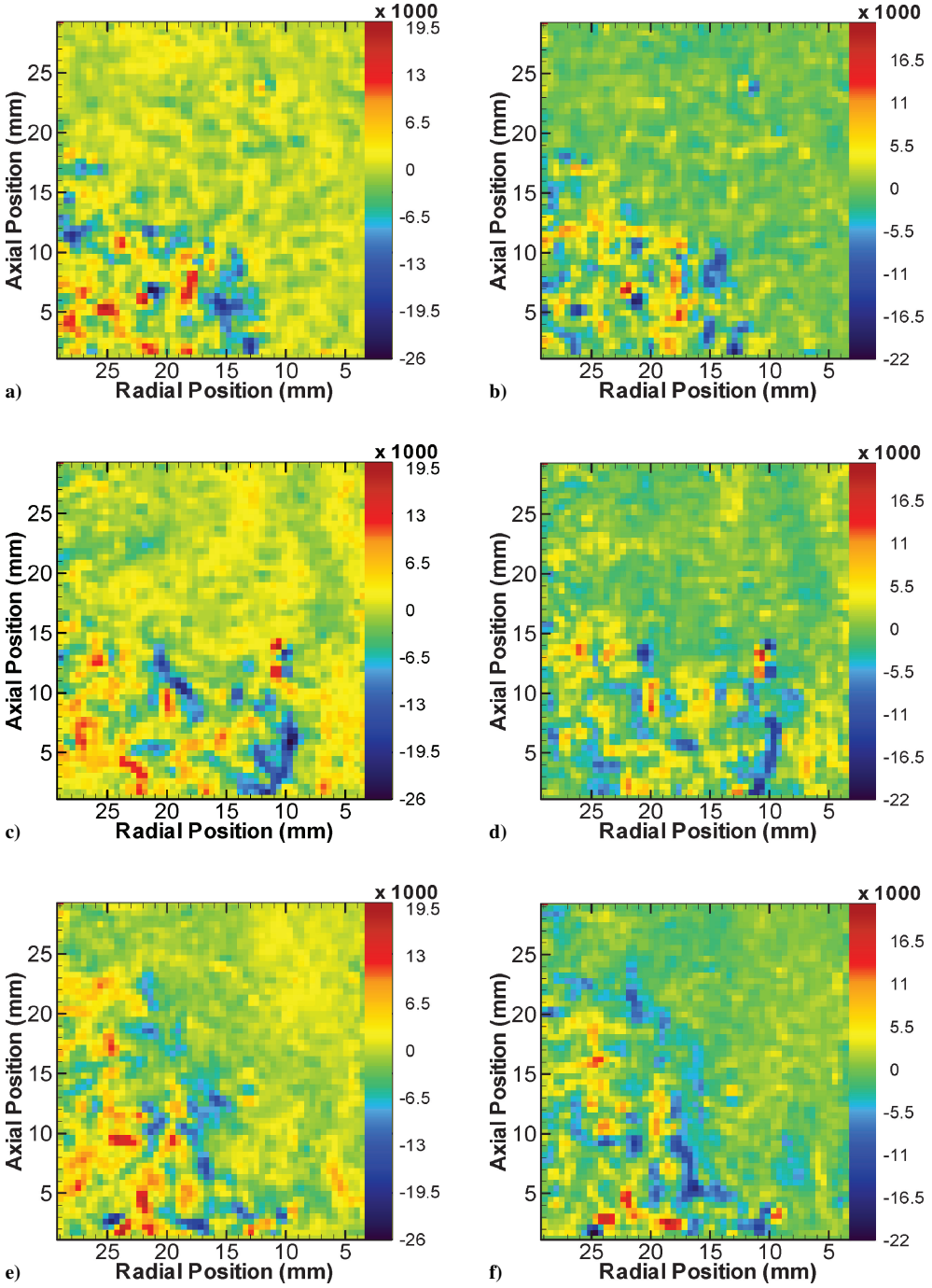

Fig. 9 Vorticity (left column) and normal strain (right column) plots of the instantaneous velocity fields shown in the left column of Fig. 4 in units of 1/s: a) and b) nonreacting case, c) and d) CH_4 flame, and e) and f) H_2-enriched flame.

the heat release. Figure 8f shows the average normal strain of the H_2-enriched flame. The regions of compression and expansion have shifted upward in conjunction with the shear layer. The peak values are 4000 s^{-1} in compression and 3000 s^{-1} in expansion. The higher extensional strain indicates more intense volumetric heat release for the H_2-enriched flame.

As shown above, the average-velocity field does not fully represent the instantaneous flowfield with smaller vortical structures. It is therefore important to consider the influence of instantaneous vorticity and normal strain on flame properties in localized regions. Figure 9 shows the instantaneous-vorticity and normal-strain fields corresponding to the velocity fields in the left column of Fig. 4. The instantaneous-vorticity field of the nonreacting flow in Fig. 9a shows random structures with peak values that are several times higher than the average values in Fig. 8. The peak vorticity magnitudes occur in the smaller structures that are absent in the time-averaged field. Instantaneous peak values are about 25,000 s^{-1} compared to peak values of 5000 s^{-1} in the averaged field. Most of the structures with positive vorticity are located in the corner recirculation zone, whereas the majority of negative-vorticity structures occur in the inner shear layer. Figure 9c shows that the instantaneous-vorticity field of the CH_4 flame is similar to that of the nonreacting flow, with matching peak values. Similar trends are observed for the instantaneous-vorticity field of the H_2-enriched flame in Fig. 9e, although the region containing positive vortical structures has shifted downstream.

The instantaneous-normal-strain field for the nonreacting case in Fig. 9b shows several small structures with regions of expansion in the inlet jet and regions of compression in the shear layers. Similar observations are made from the instantaneous-normal-strain field for the CH_4 flame in Fig. 9d and the H_2-enriched flame shown in Fig. 9f. Peak values of the instantaneous-normal-strain fields are similar for all three cases, 21,000 in expansion and 22,000 in compression. The vorticity and normal strain of the instantaneous-velocity fields are significantly different from those of the time-averaged-velocity fields. Specifically, the peak instantaneous values are several times higher than the peak mean values, and the field contains smaller random structures. Local flame extinction will depend upon the instantaneous strain rates, which were four to seven times greater than the average strain rates typically used for the analysis.

Conclusions

The two-dimensional instantaneous-velocity field of an enclosed swirl-stabilized combustor was measured using particle-image velocimetry. Measurements were taken for (a) nonreacting flow, (b) CH_4 flame, and (c) H_2-enriched CH_4 flame with the following results:

1) The time-averaged flowfield was affected not only by combustion but also by fuel composition. In particular, the addition of H_2 to CH_4 changes the orientation of the inlet jet, indicating changes in the location and rates of heat release with different fuels.

2) The size of the central recirculation zone was not significantly affected by combustion or H_2 addition to CH_4. This result differs from unconfined flows that allow thermal expansion in the radial direction to produce a wider recirculation region in reacting flows.

3) The instantaneous flowfields contained smaller, random vortical structures that were not observed in the time-averaged flowfields. The maximum velocity magnitude in the instantaneous fields was similar to that in the averaged fields.

4) Regions with high rms velocity matched with regions of high mean velocity. The CH_4 flame contained a broad region of high rms velocity and turbulent kinetic energy in the inlet jet, suggesting unsteady heat release. The maximum kinetic energy was not affected significantly by either combustion or fuel composition, possibly because of the confinement. The kinetic-energy dissipation field showed strand-shaped structures in the corner-recirculation and inlet-jet regions for all the three cases.

5) The instantaneous vorticity and normal strain were four to seven times higher than the average values. The highest magnitude was not affected significantly by combustion or hydrogen addition.

Acknowledgments

This research was supported in part by the Energy Efficiency and Renewable Energy, Hydrogen, Fuel Cells and Infrastructure Technologies Program of the Department of Energy. The experiments were conducted at the Combustion Research Facility of the Sandia National Laboratories in Livermore, California.

References

[1]Anderson, D. N., "Effect of Hydrogen Injection on Stability and Emissions of an Experimental Premixed Prevaporized Propane Burner," NASA TM X-3301, Oct. 1975.

[2]Morris, J. D., Symonds, R. A., Ballard, F. L., and Banti, A., "Combustion Aspects of Application of Hydrogen and Natural Gas Fuel Mixtures to MS9001E DLN-1 Gas Turbines at Elsta Plant, Terneuzen, The Netherlands," American Society of Mechanical Engineers, Paper 98-GT-359, 1998.

[3]Nguyen, O., and Samuelson, S., "Effect of Discrete Pilot Hydrogen Dopant Injection of the Lean Blowout Performance of a Model Gas Turbine Combustor," American Society of Mechanical Engineers, Paper 99-GT-359, 1999.

[4]Ren, J. Y., Qin, W., Egolfopoulos, F. N., and Tsotsis, T. T., "Strain Rate Effects on Hydrogen-Enhanced Lean Premixed Combustion," *Combustion and Flame*, Vol. 124, No. 4, 2001, pp. 717–720.

[5]Jackson, G. S., Sai, R., Plaia, J. M., Boggs, C. M., and Kiger, K. T., "Influence of H_2 on the Response of Lean Premixed CH_4 Flames to High Strained Flows," *Combustion and Flame*, Vol. 132, No. 3, 2003, pp. 503–511.

[6]Schefer, R. W., Wicksall, D. M., and Agrawal, A. K., "Combustion of Hydrogen-Enriched Methane in a Lean Premixed Swirl-Stabilized Burner," *Proceedings of The Combustion Institute*, Vol. 29, 2002, pp. 843–851.

[7]Ji, J., and Gore, J., "Flow Structure in Lean Premixed Swirling Combustion," *Proceedings of the Combustion Institute*, Vol. 29, 2002, pp. 861–867.

[8]Archer, S., and Gupta, A. K., "Effect of Swirl on Flow Dynamics in Unconfined and Confined Gaseous Fuel Flames," AIAA Paper 2004-0813, 2004.

[9]Griebel, P., Schären, R., Siewert, P., Bombach, R., Inauen, A., and Kreutner, W., "Flow Field and Structure of Turbulent High Pressure Premixed Methane/Air Flames," American Society of Mechanical Engineers, Paper GT-2003-38398, June 2003.

[10]Rehm, J. E., and Clemens, N. T., "The Association of Scalar Dissipation Rate Layers and OH Zones with Strain, Vorticity, and 2-D Dilatation Fields in Turbulent Nonpremixed Jets and Jet Flames," AIAA Paper 99-0676, 1999.

[11]Han, D., and Mungal, M. G., "Simultaneous Measurements of Velocity and CH Distributions. Part 1: Jet Flames in Co-Flow," *Combustion and Flame*, Vol. 132, No. 3, 2003, pp. 565–590.

[12]Gupta, A. K., Lilley, D. G., and Syred, N., *Swirl Flows*, Abacus Press, Tunbridge Wells, England, U.K., 1984, p. 4.

[13]Han, D., and Mungal, M. G., "PIV Lab 2000," ver. 1.50, Dept. of Mechanical Engineering, Stanford Univ., Stanford, CA, 2000.

[14]Raffel, M., Willert, C., and Kompenhans, J., *Particle Image Velocimetry: A Practical Guide*, Springer, New York, 1984, pp. 157–166.

[15]Haste, M. J., *An Investigation of In-Cylinder Flow and Combustion in a Spark Ignition Engine Using Particle Image Velocimetry*, Ph.D., Dissertation, Dept. of Aeronautical and Automative Engineering, Loughbourough Univ., Leicestershire, England, U.K., 2000.

[16]Peters, N., "The Turbulent Burning Velocity for Large-Scale and Small-Scale Turbulence," *Journal of Fluid Mechanics*, Vol. 384, 1999, pp. 107–132.

[17]Tsurikov, M. S., and Clemens, N. T., "The Structure of Dissipative Scales in Axisymmetric Turbulent Gas-Phase Jets," AIAA Paper 2002-0164, 2002.

Color reproductions courtesy of Sandia National Laboratories.